ACS OMEGA

http://pubs.acs.org/journal/acsodf

Article

Preparation, Characterization, and Biological Testing of Novel Magnetic Nanocomposite Hydrogels

Jianghong Huang,* Yujie Liang, Zhiwang Huang, Jianyi Xiong, and Daping Wang*

Cite This: *ACS Omega* 2020, 5, 9733−9743

Read Online

ACCESS | Metrics & More | Article Recommendations | Supporting Information

ABSTRACT: To provide a novel approach for the clinical treatment of cartilage tissue defects, we prepared a new type of magnetic nanocomposite hydrogel with an optimal raw material ratio using Fe_3O_4, polyvinyl alcohol (PVA), and type-II collagen (COLII). Briefly, five groups of PVA and collagen hydrogel matrices with different mass ratios were prepared by a combination of repeated thawing cycles and foam-frozen ice crystal separation methods. Microscopic characterization was conducted using electron microscopy, and the biomechanical properties of each group of hydrogels were then tested. The highest performing component hydrogel matrix was selected after which Fe_3O_4 with different mass ratios was introduced to construct a new Fe_3O_4/PVA/COLII hydrogel. The prepared composite hydrogels were also microscopically characterized using electron microscopy along with scanning, measurements for porosity and moisture content, and biomechanical, infrared spectrum and degradation performance testing. CCK-8 detection and staining to determine the amount of living and dead cells were also performed. Collectively, these results showed that PVA/COLII,95:5 was the optimal hydrogel matrix. Using this hydrogel matrix, five groups of composite hydrogels with different Fe_3O_4 mass ratios were then prepared. There was no significant difference in the microscopic characteristics between these different hydrogels. Fe_3O_4/PVA/COLII,5:95:5 had better physical properties as well as swelling performance and cell compatibility. The PVA/COLII,95:5 hydrogel matrix was determined to be the best, while the new magnetic nanocomposite hydrogel Fe_3O_4/PVA/COLII,5:95:5 had good, comprehensive properties.

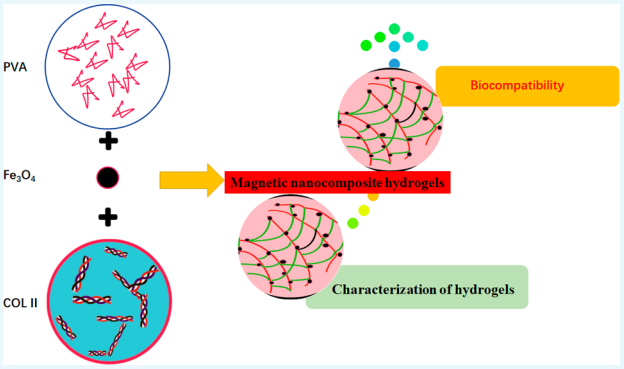

1. INTRODUCTION

Cartilage tissue damage occurs when the normal physiological structure of cartilage tissue is destroyed. During the course of this damage, the cartilage surface is initially thinned by mechanical stress, which then ruptures and leaves the tissue with minimal integrity. This type of damage is one of the most common diseases encountered in clinical orthopedics.[1] Fortunately, there are several treatment options for cartilage damage. A mild, grade I cartilage injury may use a more conservative treatment approach, including fixation, analgesia, and the use of drugs that promote cartilage tissue repair. For grades II and III damage, arthroscopic microfracture techniques and autologous cartilage transplantation techniques may be used. Despite the ability to use surgical treatment for more serious types of damage,[2] its efficacy needs to be improved. This is especially true for autologous cartilage transplantation, which requires patients to sacrifice their own healthy cartilage tissue.

Cartilage tissue engineering provides a new approach for the treatment of cartilage tissue damage.[3] In principle, this approach uses a biomimetic scaffold material that carries seed cells. This scaffold is then placed in the damaged area after which the seed cells divide and differentiate into cartilage tissue. Ultimately, these cells reach their target and allow for cartilage repair. Given this approach, there are three basic elements to cartilage tissue engineering: seed cells, scaffold materials, and cytokines to indicate the direction for healthy cells to migrate. These three elements have served as basic areas of regenerative medicine research where efforts have focused on their optimization.[4] Bifunctional, biomimetic scaffold materials are a critical part of tissue engineering research and require nontoxicity along with good histocompatibility and biomechanical properties.[5]

Collagen acts as a major component of the extracellular matrix and has good cytocompatibility.[6] Collagen hydrogels have been explored but suffer from a lack of mechanical strength and poor heat resistance. To counter this, studies have shown that a composite collagen hydrogel prepared either (1)

Received: November 30, 2019
Accepted: April 9, 2020
Published: April 20, 2020

https://dx.doi.org/10.1021/acsomega.9b04080
ACS Omega 2020, 5, 9733−9743

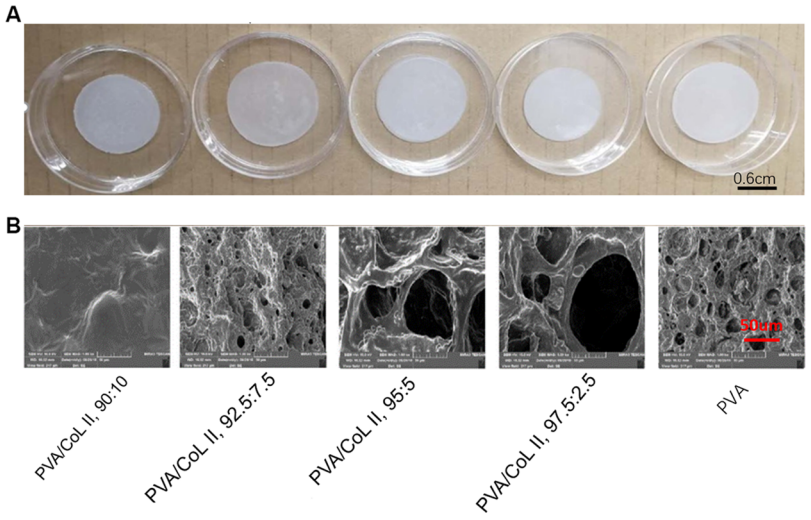

Figure 1. (A) Unmagnified view of the hydrogel matrices. (B) Electron microscopy of the hydrogel matrix, (1000×). Most of the groups (PVA/COLII,92.5:7.5, PVA/COLII,95:5, PVA/COLII,97.5:2.5, PVA) all showed loose porosity in their respective microscopic morphology features; no obvious porous structure was observed in group PVA/COLII,90:10.

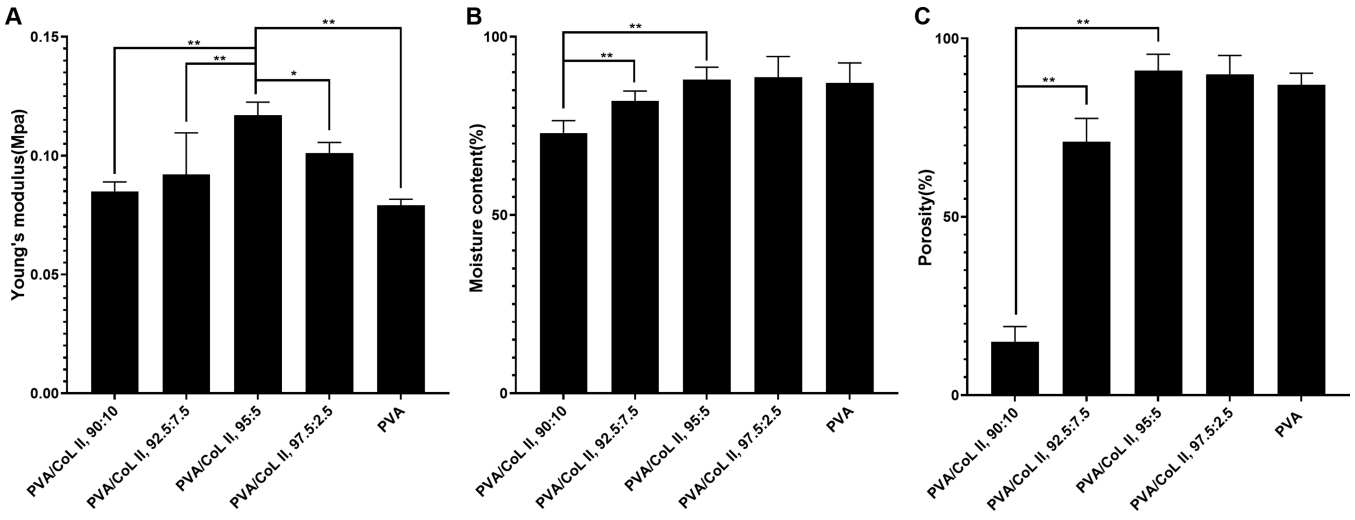

Figure 2. (A) Young's modulus diagram of the hydrogel matrix. The Young's modulus index of PVA/COLII,95:5 was significantly higher than the other groups (*$P < 0.05$, **$P < 0.01$). (B) Water contents of each hydrogel group being > 70% or more; water contents of PVA/COLII,95:5, PVA/COLII,97.5:2.5, and PVA being >85%. There was no statistically significant difference between these groups ($P > 0.05$). The water contents of PVA/COLII,90:10 and PVA/COLII,92.5:7.5 were less than the other groups. There were significant statistical differences (**$P < 0.01$) between these other groups. (C) The porosities of PVA/COLII,95:5, PVA/COLII,97.5:2.5, and PVA were all >85%; none were significantly different from each other ($P > 0.05$). The porosities of PVA/COLII,90:10 and PVA/COLII,92.5:7.5 were significantly less than those of the other groups (**$P < 0.01$).

by appropriately reducing the collagen content in the composite hydrogel or (2) by modifying the collagen provides greater cellular benefits along with better growth and biomechanical properties.[7,8] PVA is a synthetic, nontoxic biomacromolecule material with good biomechanical properties and is already widely used in various medical fields.[9,10] Given its broad medical use, it has potential for wider applications. Nanosized Fe_3O_4 particles have superparamagnetic and magnetic responsiveness, can be aggregated and positioned under specific magnetic field conditions, and generate heat after receiving electromagnetic waves. Moreover, nanosized Fe_3O_4 particles have good cell surface binding ability. Previous work has shown that magnetic nanoparticles can both regulate and promote the proliferation and differentiation behavior of bone marrow mesenchymal stem cells. Finally, these particles have also been shown to promote cartilage repair.[11,12]

Here, five sets of composite collagen hydrogel matrices for screening PVA and COLII were prepared using Fe_3O_4, PVA, and COLII as raw materials. Microscopic characterization and biomechanical tests were conducted using electron microscopy, and the results were used to select the appropriate concentrations of PVA and COLII. PVA/COLII,95:5 was chosen as the hydrogel matrix to synthesize a novel magnetic nanocomposite hydrogel; after this, five new magnetic nanocomposite hydrogel biomimetic scaffolds with different Fe_3O_4 concentrations were successfully prepared and tested. Microscopic characterization, biomechanical property assessments, and measurements regarding porosity, water content, and cell compatibility were all conducted.[13] The results of this

https://dx.doi.org/10.1021/acsomega.9b04080
ACS Omega 2020, 5, 9733−9743

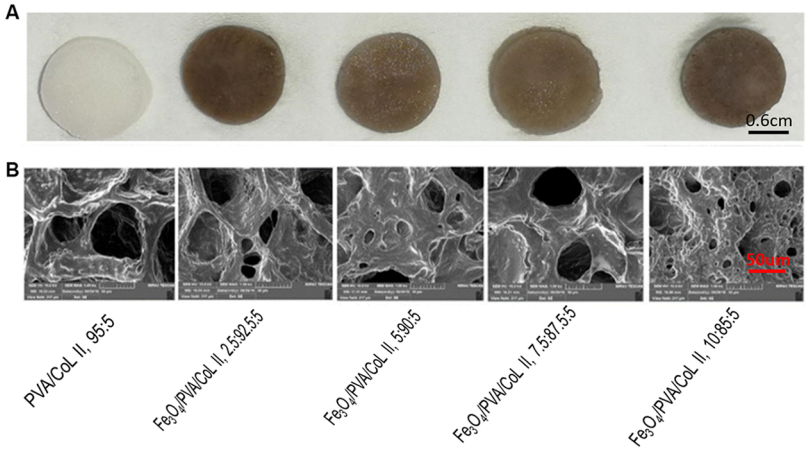

Figure 3. (A) Unmagnified view of the magnetic nanocomposite hydrogels with different Fe_3O_4 contents. (B) Electron microscopy of magnetic nanocomposite hydrogels with different Fe_3O_4 contents (1000×). All of the samples with different Fe_3O_4 contents had loose, porous micromorphological characteristics. There were no significant differences in these characteristics between groups.

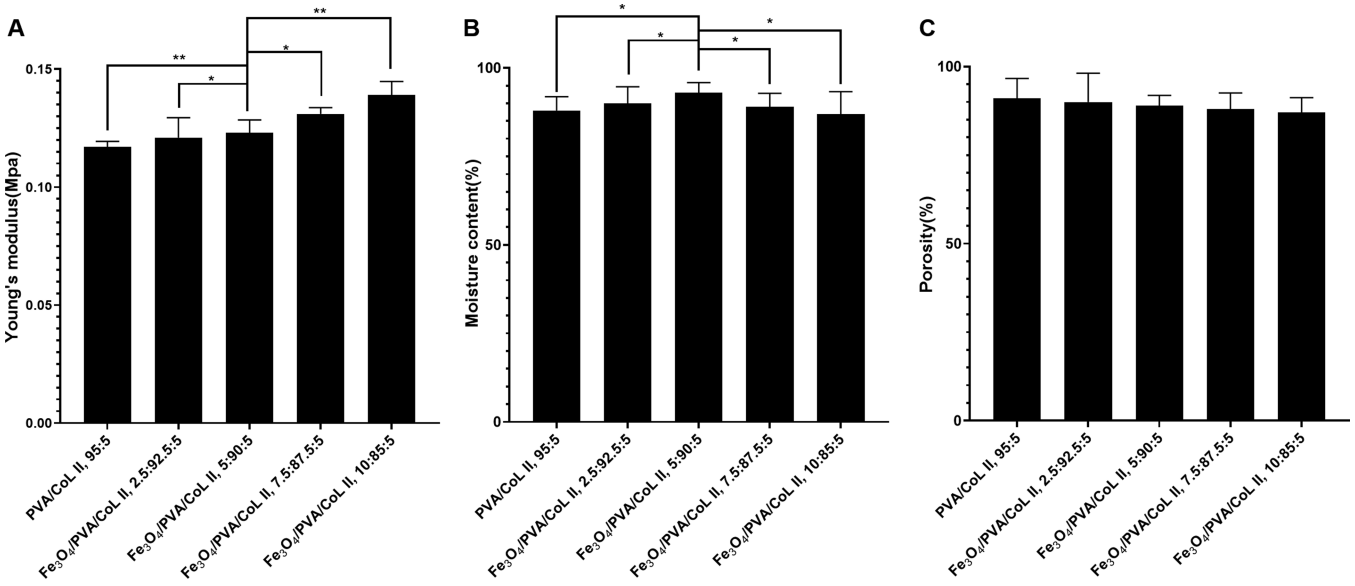

Figure 4. (A) Young's modulus diagram of the magnetic nanocomposite hydrogel. In the new magnetic nanocomposite hydrogel, increasing the Fe_3O_4 content resulted in a corresponding increase in the Young's modulus index and stronger antideformation characteristics and biomechanics. Stronger performers were statistically different ($^*P < 0.05$, $^{**}P < 0.01$). (B) Water content of the magnetic nanocomposite hydrogels with different Fe_3O_4 contents. The water content of each magnetic nanocomposite hydrogel group with different Fe_3O_4 contents were all above 85%. The water content of Fe_3O_4/PVA/COLII,5:90:5 was significantly higher than the other tested groups ($^*P < 0.05$). (C) Porosity of magnetic nanocomposite hydrogels with different Fe_3O_4 contents. The porosities of each magnetic nanocomposite hydrogel group were all >80% and were not significantly different ($P > 0.05$).

work are expected to prepare future biomimetic scaffold materials for use in the clinical treatment of damaged cartilage tissue.

2. RESULTS AND DISCUSSION

2.1. Performance Test Results for the Prepared Hydrogel Matrix. Three samples were randomly selected from each group for scanning electron microscopy. Most groups (PVA/COLII,92.5:7.5, PVA/COLII,95:5, PVA/COLII,97.5:2.5, PVA) showed loose, porous, microscopic features along with loose porous network structures. The macro- and micropores were interspersed in this arrangement. Pore diameters ranged from 10 to 100 μm; in some cases, the pore diameter was more than 20−50 μm. No obvious porous structure was observed in the PVA/COLII,90:10 group (Figure 1B).

A sample of each group's hydrogel matrix was randomly selected for the Young's modulus index test to determine their respective mechanical properties. Figure 2A shows the Young's modulus model of each set of hydrogel matrices. As shown, a decrease in COLII content resulted in an initial, gradual increase in the Young's modulus index of the hydrogel matrix, including the Young's modulus index of group PVA/COLII,95:5. After peaking, the Young's modulus index of the hydrogel matrix then decreased with a decrease in COLII mass. In all data shown, $P < 0.05$ indicated a statistically significant difference.

As shown in Figure 2B, water content test results indicated that an increase in COLII content resulted in an initial increase

https://dx.doi.org/10.1021/acsomega.9b04080
ACS Omega 2020, 5, 9733−9743

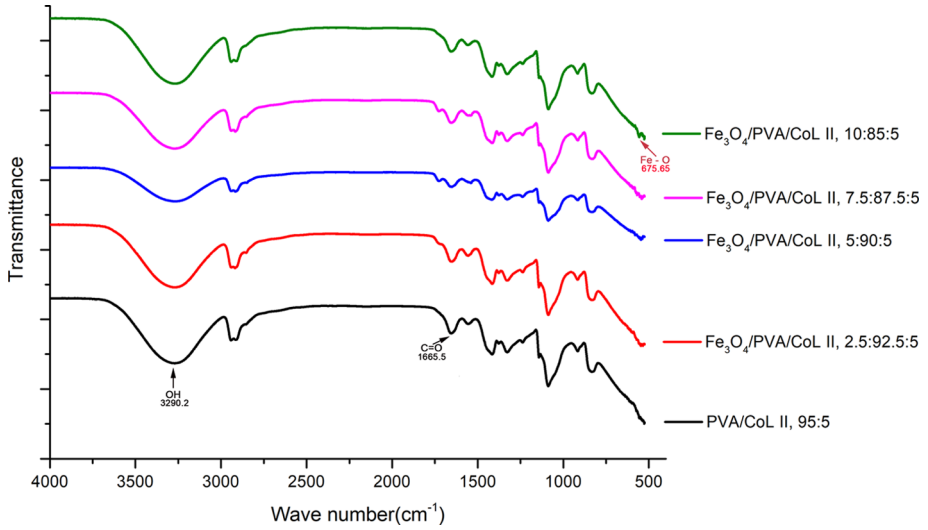

Figure 5. Infrared spectrum of the magnetic nanocomposite hydrogels. The infrared spectra of each group of magnetic nanocomposite hydrogels were similar, with all containing OH, C═O, and Fe−O groups that had their characteristic IR peaks. When compared with PVA/COLII,95:5, the magnetic nanocomposite hydrogel materials had the characteristic peaks of the special functional groups of Fe_3O_4.

in hydrogel matrix water content followed by a decrease. In particular, the moisture contents of groups PVA/COLII,95:5 and PVA/COLII,97.5:2.5, PVA) were all >85%. There was no statistically significant difference between these two groups (P > 0.05). The water contents of the other groups—PVA/COLII,90:10 and PVA/COLII,92.5:7.5—were lower than those of the other groups. In this case, there was a significant statistical difference (P < 0.05). Given these results, we determined that the swelling performance of group PVA/COLII,95:5 was optimal.

As shown in Figure 2C, porosity test results showed that an increase in COLII content was associated with an initial increase in the porosity of the hydrogel matrix followed by a decrease. The porosities of three groups (PVA/COLII,95:5, PVA/COLII,97.5:2.5, and PVA) were all >85%. There was no statistically significant difference between these groups (P > 0.05). The porosities of the other groups—PVA/COLII,90:10 and PVA/COLII,92.5:7.5—were significantly less than those of the other groups. This difference was significant (P < 0.05). Our results indicated that the porosity of group PVA/COLII,95:5 was optimal.

2.2. Magnetic Nanocomposite Hydrogel Performance Test Results. Scanning electron microscopy was used to assess three randomly selected samples from each hydrogel group. Each sample had microscopic pore structures, with micropores that were uniformly distributed on the surface and the interior of the newly formed magnetic nanocomposite hydrogels. Imaging also revealed a loose porous network with large pores and interspersed micropores. Large pores had diameters ranging from 150−300 μm, while smaller pores had diameters ranging between 20−50 μm. No Fe_3O_4 particles had deposited into the hydrogel blocks. There were no significant differences in pore distribution between groups (Figure 3B).

2.2.1. Mechanical Property Test. Figure 4A shows the Young's modulus model of each magnetic nanocomposite hydrogel group. As indicated, increasing the Fe_3O_4 content results in a gradual increase in the Young's modulus index of the new magnetic nanocomposite hydrogels. This also results in a gradual increase in its antideformation ability. When a bionic scaffold material is implanted in the body, it is to be affected by the shearing and compressive forces of the surrounding tissue. If the bionic scaffold material does not have a certain capacity to resist deformation, it may be displaced—or even rupture—in the body. This would ultimately affect the therapeutic effect of the scaffold and even cause other damage. The Young's moduli of the new magnetic nanocomposite hydrogels groups were higher than those of the hydrogel matrix without Fe_3O_4, indicating that the introduction of Fe_3O_4 lent the hydrogel matrix better resistance to deformation.

We conducted our water content test by randomly selecting three samples from each magnetic nanocomposite hydrogel group. Samples that had similar appearance and dimensions related to the water content index test were selected.

The water content of each magnetic nanocomposite hydrogel group was above 80%. The water content of Fe_3O_4/PVA/COLII,5:90:5 was the highest when compared with the other groups; this difference was significant (P < 0.05; Figure 4B). Although the introduction of Fe_3O_4 has no obvious influence on the swelling properties of the new magnetic nanocomposite hydrogel, it has an effect on water content. Possible reasons behind this effect are discussed further in the Discussion section.

Three samples from each magnetic nanocomposite hydrogel group were randomly selected to use in our porosity test. Each sample had a similar appearance and dimensions related to the porosity index test. The porosity of each magnetic nanocomposite hydrogel group was above 85%, and there were no significant differences between groups (P > 0.05; Figure 4C). The introduction of Fe_3O_4 had no significant effect on the new magnetic nanohydraulic porosity index, which was consistent with our electron microscopy results.

Infrared spectroscopy was used to assess each magnetic nanocomposite hydrogel group at random points. Results show that the OH (PVA), C═O (COLII), and F−O (Fe_3O_4) were all observed in the infrared spectra of each magnetic nanocomposite hydrogel group. The presence of functional groups (Figure 5) indicated that each magnetic nanocomposite hydrogel group contained PVA, COLII, and Fe_3O_4. When compared with PVA/COLII,95:5, the magnetic nanocompo-

https://dx.doi.org/10.1021/acsomega.9b04080
ACS Omega 2020, 5, 9733−9743

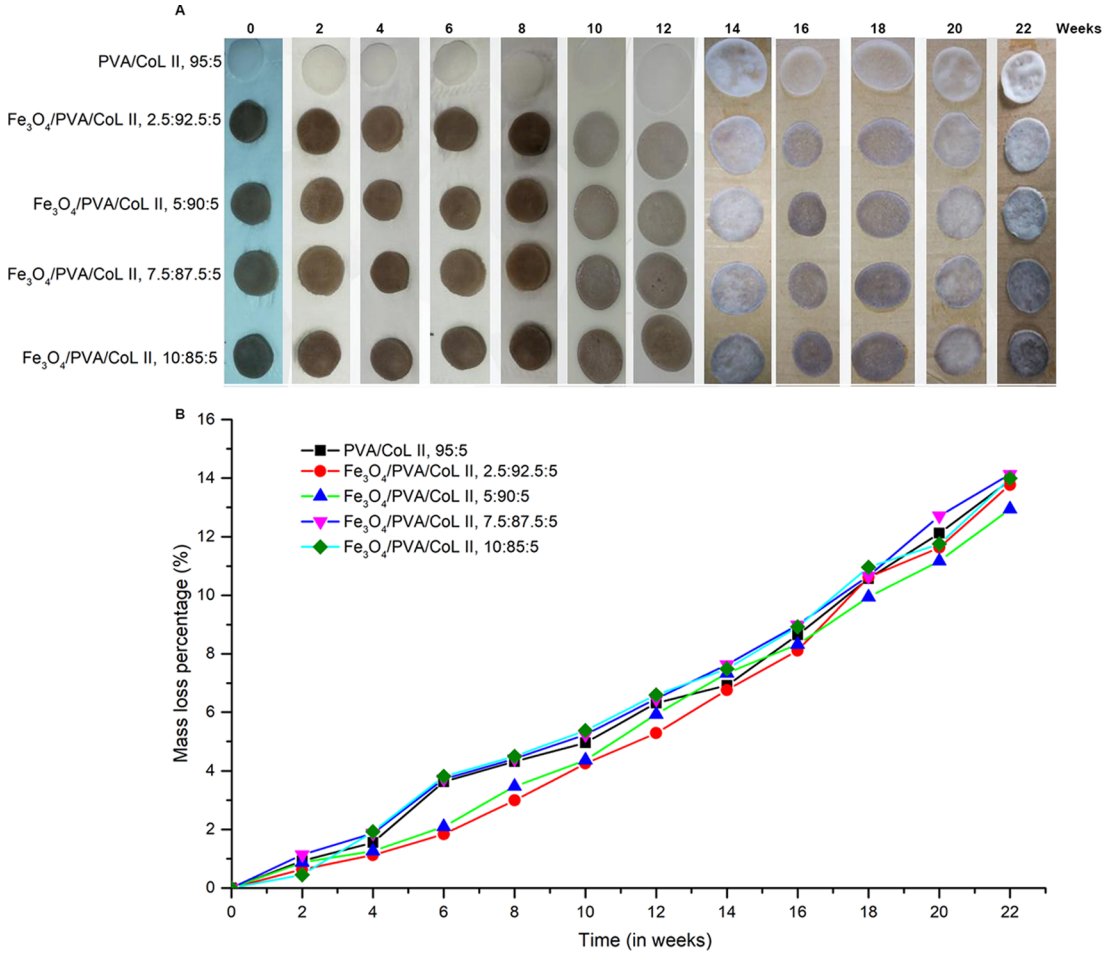

Figure 6. (A) Degradation process of the new magnetic nanocomposite hydrogel. Increased degradation time resulted in lightening and darkening of the color of each hydrogel group. Increased degradation time also resulted in hydrogel thinning. (B) With increased degradation time, the quality of each group of magnetic nanocomposite hydrogels being steadily decreased. There were no statistically significant differences in the mass loss between groups ($P > 0.05$).

site hydrogel materials had the characteristic peaks of the special functional groups seen in Fe_3O_4.

2.2.2. In Vitro Degradation Experiments. Samples from the five magnetic nanocomposite hydrogel groups were subjected to in vitro degradation experiments for 22 weeks. As shown in Figure 6A, increased in vitro degradation time resulted in lightening and darkening of the color of each group of magnetic nanocomposite hydrogels. Increased in vitro degradation time also resulted in a thinner thickness. Figure 6B shows the tested hydrogels of each group. Continuous monitoring of the mass loss ratio indicated that the quality of each magnetic nanocomposite hydrogel group was stable. Moreover, this stability was lost with increased degradation time. There were no statistically significant differences in the mass loss between groups ($P > 0.05$).

2.2.3. Living and Dead Cell Staining Experiments. BMSCs were allowed to proliferate for 7 days; afterward, staining for living and dead cells revealed green fluorescence from living cells. The cellular proliferation of each group was well differentiated, and there were different degrees of cell proliferation. The live cells from Fe_3O_4/PVA/COLII,5:90:5 had a large number of cells with regular, cell stacking growth (Figure 7A). Cell proliferation was also superior relative to other groups, indicating that Fe_3O_4/PVA/COLII,5:90:5 had better cell compatibility than the other tested groups.

2.2.4. CCK-8 Cell Proliferation Assay. Three samples from each magnetic nanocomposite hydrogel group were randomly selected for CCK-8 cell proliferation experiments (Figure 7B). Rabbit bone marrow mesenchymal stem cells were introduced to each group of magnetic nanocomposite hydrogels after which they survived and proliferated. On the first day after cell inoculation, there were no significant differences in cell proliferation between groups ($P > 0.05$). On the 3rd and 7th days, the bone marrow mesenchymal stem cells proliferated to a large degree. Moreover, the bone marrow mesenchymal stem cells that were inoculated on the Fe_3O_4/PVA/COLII,5:90:5 hydrogel were the most active when compared with the other groups. This difference was significantly higher than all other tested groups ($P < 0.05$).

2.3. Discussion. The joint cavity is a relatively closed, hypoxic microenvironment, and the distribution of blood vessels and nerves in the cartilage of the joint surface is notably decreased. Cartilage tissue damage has always been a major problem in both basic and clinical orthopedic research.[14,15] One promising treatment for cartilage tissue damage has been cartilage tissue engineering, which uses seeded cells onto biocompatible stents.[16,17] In such cartilage tissue engineering, there are innumerable reports using various types of collagen-based composite hydrogels.[18,19] However, no artificial biomimetic scaffold material has yet been shown to be

https://dx.doi.org/10.1021/acsomega.9b04080
ACS Omega 2020, 5, 9733−9743

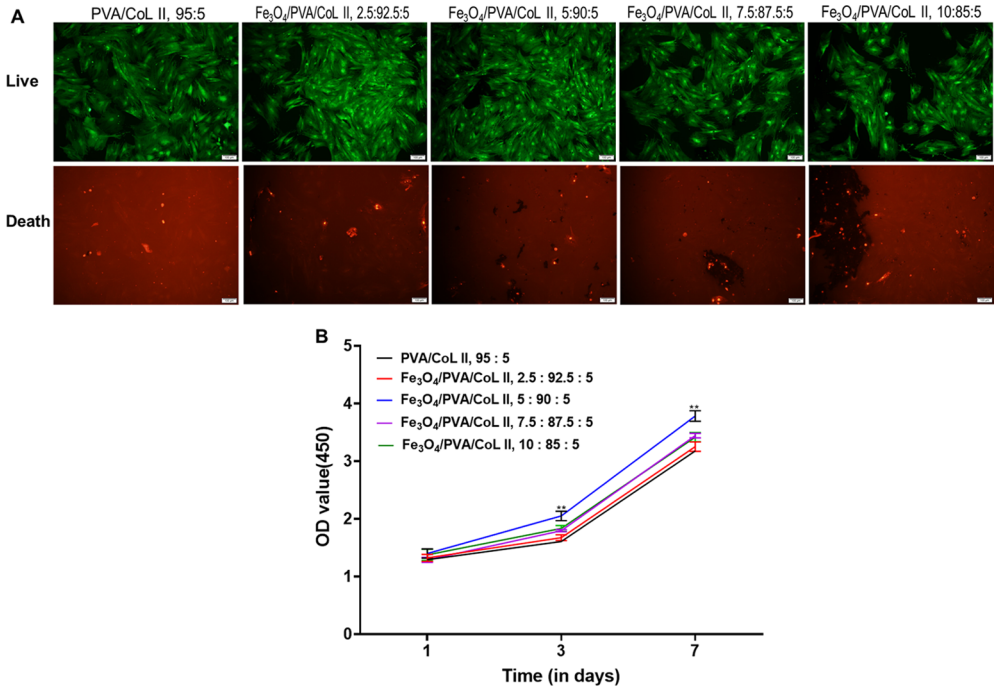

Figure 7. (A) Staining for living and dead cells on magnetic nanocomposite hydrogels with different Fe_3O_4 contents after 7 days of cell culture. Cells were inoculated in samples from each group; after inoculation, all cells proliferated well. The cell proliferation of the Fe_3O_4/PVA/COLII,5:90:5 group was better than that of the other groups. (B) CCK-8 cellular proliferation results from magnetic nanocomposite hydrogels with different Fe_3O_4 contents. Cells were inoculated on each group, survived, and proliferated. On the third day after inoculation, the cell proliferation of Fe_3O_4/PVA/COLII,5:90:5 was notably better than the other tested groups. This difference was significant until the 7th day after inoculation (*P < 0.05, **P < 0.01).

equivalent to natural cartilage in terms of its biomechanical properties.[20]

Here, PVA and type-II collagen were used as raw materials, and five groups of hydrogel matrix biomimetic scaffolds with different composition ratios were prepared by a physical cross-linking method of repeated freeze−thaw and surfactant foaming techniques (Figure 1A). A group of hydrogel matrices with an optimal ratio of PVA and COLII was screened using microscopic scanning and biomechanical testing under electron microscopy. Based on the resulting hydrogel matrix from this initial testing, five groups of hydrogels with new magnetic properties were prepared using different Fe_3O_4 concentrations, resulting in new magnetic nanocomposite hydrogels (Figure 3A).

The bionic scaffold materials of each group did not show any obvious microscopic morphological differences under electron microscope scanning, and all had many microporous structures. The reason for this similarity may have been because the ratio of polysorbate 80 surfactant introduced into each group was the same. The pore formation of each hydrogel group was primarily dependent on the bubbles generated by the polysorbate 80 surfactant during the stirring process during the early stage of the preparation process and had nothing to do with the contents of Fe_3O_4, PVA, or COLII. Prior to any experiments, a hydrogel of the same composition ratio that did not have any polysorbate 80 was prepared. A large amount of microporous structures was observed using electron microscopy. The fixation ratio of polysorbate 80 surfactant has been shown to determine the stability of the hydrogel's pore structure.[21] This is consistent with the porosity test results of each hydrogel group. In our water content testing, Fe_3O_4/PVA/COLII,5:90:5 was the magnetic nanocomposite hydrogel that had the highest water content relative to other hydrogels. This difference was significant (P < 0.05). The existence of Fe_3O_4 particles was not directly observed using electron microscopy. On the one hand, the magnetic nanoparticles were uniformly distributed and not aggregated. On the other, the uniform distribution of Fe_3O_4 nanoparticles may have resulted in an amount of hydrophilicity in the hydrogel matrix. Each group also had different water contents. The hydrogel matrix showed stronger hydrophilicity in the case of the Fe_3O_4 ratio found in the group Fe_3O_4/PVA/COLII,5:90:5. Excessive nanoparticles may clog the hydrogel when the Fe_3O_4 ratio increases too much. When coupled with the tiny pores in the hydrogel, the water carrying capacity of the hydrogel would drop.[22]

The polysorbate 80 surfactant is toxic,[23] and it was subjected to multiple rounds of soaking in ultrapure water prior to all CCK-8 and cell staining experiments. Despite this, it is difficult to ensure that there was no small amount of remaining residue. However, any potential polysorbate 80 surfactant residue and the hydrogel's pore structure are easy problems to solve.[24] The selection of polysorbate 80 surfactant in the preparation process should be done to ensure sufficient pore formation and to allow for a standard structure.[25]

Due to their good histocompatibility and low immunogenicity, hydrogels have inherent advantages in medical research and application. The introduction of magnetic particle materials makes the hydrogels responsive to magnetic fields, which is in line with current medical science and the increasing demand for medical materials to be intelligent and controllable. In addition to the development of magnetic hydrogels for use in bone and cartilage tissue engineering, they have also been explored in the fields of tibia healing,[26] artificial

https://dx.doi.org/10.1021/acsomega.9b04080
ACS Omega 2020, 5, 9733−9743

muscles,[27] and osteomyelitis treatment.[28] Moreover, the magnetic influence of magnetic hydrogels when combined with chemotherapeutic drugs has also been explored to achieve controlled and targeted transport and release of bone and cartilage tumor treatment drugs.[29] This area of research requires additional attention and exploration, with one of the larger problems being the difficulty in effectively passing the drug from the magnetic hydrogel through the denser bone and cartilage tissue into the target area. Of note is the fact that there is a contradiction between the deformation ability of the magnetic hydrogel and its mechanical strength. This highlights the importance of the selection and proportion of component materials, as well as the need for further research and improvement. The development of interdisciplinary research, 3D printing technology,[30,31] ceramic materials,[32] and other related disciplines is expected to be combined with magnetic hydrogel research. This will provide a fruitful intersection in the research and application of magnetic hydrogels—particularly in bone and cartilage tissue engineering.[33−39] The magnetic field reactivity of Fe_3O_4 was retained in our novel magnetic nanocomposite hydrogel. Although the Fe_3O_4 content was low in each magnetic nanocomposite hydrogel group, each was able to be attracted by magnets and there was no decrease in this ability (Figure S3). This finding indicated that all groups had strong magnetic field responsiveness.

Since the preparation of biomimetic scaffold materials for cartilage tissue engineering involves the use of raw materials, component ratio adjustment, pre-experiment, and performance testing, it is a very large system engineering problem. As a result, there are limitations here that will require further exploration, including (1) decreased groups and adjustment and further refinement of the composition ratio, (2) better understanding of the distribution of bone marrow mesenchymal stem cells inside the new magnetic nanocomposite hydrogel, and (3) further in vivo experiments to confirm the repair effect on cartilage tissue damage of the new magnetic nanocomposite hydrogels.

3. CONCLUSIONS

Here, microscopic characterization, biomechanical properties, water content, porosity, infrared spectroscopy, in vitro degradation, CCK-8 and cell staining of five groups of hydrogel matrix biomimetic scaffolds and novel magnetic nanocomposite hydrogels were tested. The experimental results showed that PVA/COLII,90:5 was the best-performing hydrogel matrix bionic scaffold material. Fe3O4/PVA/COLII,5:90:5 emerged as a new type of magnetic nanocomposite hydrogel with the best comprehensive performance, including in terms of its microscopic pore structure, biomechanical and swelling properties, and cell compatibility. Future experiments will be needed regarding cell proliferation and in vivo testing to further evaluate the feasibility of these new magnetic nanocomposite hydrogels for use in cartilage tissue engineering.

4. MATERIALS AND METHODS

4.1. Main Materials and Reagents. Main materials and reagents used are as follows: Magnetic nanoparticles (Fe_3O_4) (Jiangsu Xianfeng Nanomaterials Technology Co., Ltd.) and polyvinyl alcohol (PVA) (Changchun Chemical Co., Ltd.) were obtained from their respective companies. Type-II collagen (COLII), DMEM cell culture medium, PBS buffer, fetal calf serum, double antibody, and 1‰ FGF were all obtained from Gibco (USA). The polysorbate 80 surfactant was from Sigma, USA, and 75% and 95% medical-grade alcohol were purchased from Fujian Province III Lin Pharmaceutical Co., Ltd. A commercially available CCK-8 kit was obtained from Biyuntian Biotechnology Co., Ltd.

Equipment included an electronic balance (Fangrui Company, Shanghai, China), electronic universal ability testing machine (Shenzhen Suns Industrial Instrument Company), DSC Q100 system (TA Company, USA), magnetic stirrer (IKA Company, Germany), freeze dryer (Beijing Sihuan Precision Instrument Company), cell incubator (Thermo Company, USA), scanning electron microscope (TESCAN Company, Czech Republic), infrared spectrometer (Neaspec, Germany), fluorescence inverted microscope (Leica, Germany), and pH tester (Shanghai Lichen Technology Co., Ltd.).

4.2. Experimental Methods. *4.2.1. Preparation of the Hydrogel Matrix.* Ten grams of PVA was weighed and placed in 90 mL of ultrapure water. The resulting mixture was sealed and placed on a magnetic stirrer (60 °C, 30 min). The magnetic stirrer remained engaged at a rotation speed of 600 rpm, and the solution was heated to 90 °C. The solution was stirred for 3 h until a transparent viscous mass formed with a ratio of 10% PVA solution (liquid A). Liquid A was stored at 90 °C until later use. COLII (1.00 g) was dissolved in 99 mL of ultrapure water, heated to 40 °C, and stirred for 60 min to form a viscous translucent mass with a ratio of 1% COLII solution (liquid B). Liquid B was stored at 40 °C until later use.

Liquids A and B were mixed in different volume ratios; more specifically, 10, 7.5, 5.0, 2.5, or 0 mL of Liquid B were separately added to 10 mL of Liquid A and designated as follows: PVA/COLII,90:10, PVA/COLII,92.5:7.5, PVA/COLII,95:5, PVA/COLII,97.5:2.5, and PVA. Each solution was then sealed, heated to 40 °C, and stirred at 600 rpm for 2 h. The mixture was thoroughly mixed until it formed a viscous, translucent homogeneous liquid. A few drops of polysorbate 80 surfactant were added dropwise to each solution at a volume ratio of 100:1. The resulting solutions were separately sealed, heated to 40 °C, and stirred at 600 rpm for 30 min until each solution was thoroughly mixed. The resulting solutions were then individually transferred to a 24-well culture plate and sealed for 7 freeze−thaw cycles (−20 °C for 16 h/room temperature for 8 h).[40] The resulting hydrogel matrices were divided into two batches: One batch was stored in ultrapure water at room temperature, and the second (3 mm thickness) was vacuum freeze-dried to remove any water. All matrices were then stored in a dry environment until later experiments.

4.2.2. Performance Test of Hydrogel Matrices. 4.2.2.1. Scanning Electron Microscopy. The surface of each hydrogel matrix group sheet was vacuum-dried and sprayed with gold. Electron microscopy was then used to determine the three-dimensional structure of the pore morphology of each type of hydrogel matrix.

4.2.2.2. Mechanical Property Test. The mechanical properties of each group of hydrogel matrices (Figure S1A) were tested with a uniform shape of each type of hydrogel matrix using an electronic versatility tester. The uniform shape of each hydrogel matrix was cylindrical with a diameter of 12 mm and a height of 6 mm. The compression speed of the electronic universal testing machine was 2 mm/min. Each group was tested with five monomer samples, and the hydrogel matrix

https://dx.doi.org/10.1021/acsomega.9b04080
ACS Omega 2020, 5, 9733−9743

was compressed according to the national standard (stress and strain capacity indicators).

4.2.2.3. Moisture Content. Each type of hydrogel matrix was cut with a blade into a cylinder with a diameter of 12 mm and a height of about 6 mm. Excess moisture on the surface of the hydrogel was dried with filter paper, and the hydrogel was then weighed using an electronic balance. The mass of each hydrogel was recorded as m_1. After weighing, each type of hydrogel matrix cylinder was placed in a vacuum freeze-drying oven for 72 h to remove all water then weighed separately on an electronic balance. This mass was recorded as m_2 and the water content was calculated as follows: $C = (m_1 - m_2)/m_1 \times 100\%$.[41] Three sets of monomer samples were used for each hydrogel matrix type and the average was used for all final results.

4.2.2.4. Porosity. Each group of hydrogel matrix was cut into a square using a blade. Each square's side length was 1 cm, with a water volume of 1 cm^3. Excess water on the surface of the hydrogel was dried with a filter paper after which it was weighed using an electronic balance. All masses were recorded as m_3. After weighing, each group of hydrogel matrix cubes was placed in a vacuum freeze-drying oven for 72 h to remove all moisture. Hydrogel matrix cubes were then weighed using an electronic balance and resulting masses were recorded as m_4. The porosity was calculated as follows: $C = (m_3 - m_4)/1 \times 100\%$.[41] Three sets of monomer samples were used for each hydrogel matrix type and the average was used for all final results.

4.2.3. Preparation of a Novel Magnetic Nanocomposite Hydrogel. The best hydrogel matrix was selected after 4.2.1 and 4.2.2 experimental procedures and was determined to be PVA/COLII,95:5. This hydrogel was used for the preparation of a novel magnetic nanocomposite hydrogel.

Five hundred milliliters of A solution and 250 mL of B solution (0.5 g of COLII dissolved in 50 mL of ultrapure water) were prepared according to the experimental protocol described in section 4.2.1. Five hundred milliliters of liquid A and 250 mL of liquid B were divided into five groups: PVA/COLII,95:5, Fe_3O_4/ PVA/COLII,2.5:92.5:5, Fe_3O_4/PVA/COLII,5:90:5, Fe_3O_4/PVA/COLII,7.5:87.5:5, and Fe_3O_4/PVA/COLII,10:85:5. The groups were determined according to the 2:1 volume ratio. After mixing liquids A and B, 150 mL of each group was added into separate A and B mixtures. All resulting solutions were then stirred using a large magnetic stirrer and sealed with disposable sealing glue. The container mouth was placed on a magnetic stirrer and heated to 40 °C. Stirring alternated between clockwise/counterclockwise motions; total stirring was 2 h and stirring was done until liquids A and B were thoroughly mixed to form a viscous, translucent shape. All solutions were mixed evenly. Fe_3O_4 nanoparticles were weighed using an electronic balance: 0, 0.25, 0.5, 0.75, or 1.00 g of Fe_3O_4 nanoparticles were added to each separate mixture and stirred continuously for 1 h using a magnetic stirrer.

After stirring, the black Fe_3O_4 nanoparticles were uniformly distributed in the hydrogel matrix. A few drops of polysorbate 80 surfactant were then added to each solution at a volume ratio of 100:1. The beaker mouth was sealed again and stirred at 40 °C for 2 h in a clockwise/counterclockwise direction using a magnetic stirrer. After stirring, each solution was more turbid than prior to the addition of polysorbate; moreover, each solution was filled with microbubbles. Each solution was mixed at 40 °C before being transferred using a disposable pipette to a 24-well culture plate. Culture plates were then covered with separate plate covers after which plates were sealed with tape to prevent water evaporation. Each group was marked and dated. The culture plate containing the mixed solution was sealed and then placed in a freezer and cross-linked using a freeze−thaw method. Briefly, the freezer was set to −20 °C and the sealed culture plate was frozen for 16 h after which it was carefully removed and maintained at room temperature to melt. After 8 h in room temperature, the plate was again placed in a freezer compartment at −20 °C for freezing. Each freeze−thaw cycle was performed once, and this freeze−thaw cycle was performed 7 times. The final hydrogel matrices that resulted were divided into two batches, with the first being stored in ultrapure water at room temperature. The second (3 mm thickness) was vacuum freeze-dried to remove any residual water and then stored in a dry environment before later experiments.

4.2.4. Thawing Cells and Culturing of Rabbit Bone Marrow Mesenchymal Stem Cells. Frozen rabbit bone marrow mesenchymal stem cells were removed from liquid nitrogen, placed in a 37 °C water bath, and shaken for 5 min to promote melting. After 30 min of UV irradiation on an an ultraclean workbench, the rabbit bone marrow mesenchymal stem cells were transferred to a 15 mL centrifuge tube using a sterile pipette on a clean bench, and another sterile pipette was used. DMEM medium (10 mL, maintained at 37 °C) was gently pipetted into the centrifuge tube. The mixture of DMEM and rabbit bone marrow mesenchymal stem cells was then centrifuged for 10 min (1000 r/min) after which the supernatant was discarded and 10 mL of DMEM (maintained at 37 °C) was added to the precipitate. Mix gently with a pipette to make it even. The mixture of DMEM and rabbit bone marrow mesenchymal stem cells was inoculated into a cell culture flask after which the cell culture was conducted in a cell culture incubator at 37 °C in a 5% CO_2 atmosphere. The next day, the culture solution was discarded, and 10 mL of DMEM (maintained at 37 °C) was added. On the third day post-inoculation, microscopy was used to determine the cell density; cell density was determined to be 80%. At this point, the culture solution was discarded and cells were washed twice with 10 mL of PBS. Afterward, 3 mL of 0.25% trypsin was added using a sterile pipette after which the cell culture was placed in an incubator for 3 min. To stop the digestion, 1 mL of DMEM was added after which cells were transferred to a 15 mL centrifuge tube with a sterile pipette. Cells were centrifuged for 10 min (1000 r/min) after which the supernatant was discarded. DMEM (10 mL, maintained at 37 °C) was gently pipetted to the precipitate. Finally, a sterile pipette was used to add 10 mL of culture medium to each group of the prepared magnetic nanocomposite hydrogels. The seeded hydrogels were then placed in an incubator at 37 °C and in a 5% CO_2 atmosphere. All cell cultures were conducted in a cell culture incubator (Figure S2A,B); the resulting seeded hydrogels were then used in later experiments.

4.2.5. Disinfection of New Magnetic Nanocomposite Hydrogel Biomimetic Scaffold Materials. The first batch of 24-well culture plates that had been loaded with each group of new magnetic nanocomposite hydrogels was removed from room temperature, ultrapure water. All excess water was removed from the hydrogels' surfaces after which they were completely immersed in medical-grade alcohol with a volume fraction of 75%. Any residual water in the hydrogels would dilute the alcohol content; as a result, the 75% medical-grade

https://dx.doi.org/10.1021/acsomega.9b04080
ACS Omega 2020, 5, 9733−9743

alcohol was replaced every 12 h and maintained at room temperature. This series of alcohol replacements was repeated for a total of three times. A sterile bag was removed from the 24-well culture plate that had been submerged in alcohol; this bag was completely immersed in sterile ultrapure water, which was changed every 3 h for 8 consecutive times. A sterile, nonalcoholic new magnetic nanocomposite hydrogel was obtained after this process. This hydrogel was sealed, and the surface of the plate was wiped with 75% alcohol until later experiments.

4.2.6. Performance Testing of New Magnetic Nanocomposite Hydrogels. 4.2.6.1. Scanning Electron Microscopy. After vacuum drying, the surfaces of the new magnetic nanocomposite hydrogels from each group were sprayed with gold. The three-dimensional structures of these novel magnetic nanocomposite hydrogels were then observed using scanning electron microscopy.

4.2.6.2. Mechanical Property Test. The new magnetic nanocomposite hydrogels from each group that had the same shape were tested using an electronic universal testing machine. This was done to assess the mechanical properties of the new magnetic nanocomposite hydrogels (Figure S1B). These new magnetic nanocomposite hydrogels had a uniform diameter of 12 mm and a height of 6 mm. The compression speed of the electronic universal testing machine was 2 mm/min. Each group was tested using five individual samples. The new magnetic nanowater was measured according to the national standard (the index of compressive stress and strain capacity of the gel).

4.2.6.3. Moisture Content. The new magnetic nanocomposite hydrogels from each group were cut into cylinders, each with a diameter of 12 mm and a height of approximately 6 mm. The excess moisture on the surface of the hydrogel was dried with filter paper, and the hydrogels were individually weighed using an electronic balance. The mass was recorded as m_1. After weighing, each hydrogel cylinder from each group was placed in a vacuum freeze-drying oven for 72 h to remove any residual water. Hydrogel cylinders were then individually weighed using an electronic balance and the mass was recorded as m_2. The water content was calculated as $C = (m_1 - m_2)/m_1 \times 100\%$.[41] Three sets of individual samples were used for each new magnetic nanocomposite hydrogel, and the averages were used for all final analyses.

4.2.6.4. Porosity. Each group of new magnetic nanocomposite hydrogels was cut into a square with a side length of 1 cm and a volume of 1 cm^3. Filter paper was used to dry any excess water from the surface of the hydrogel after which each hydrogel was individually weighed using an electronic balance, and the mass was recorded as m_3. After weighing, the new magnetic nanocomposite hydrogel cubes were placed in a vacuum freeze-drying oven for 72 h and then weighed again using an electronic balance. The mass was recorded as m_4, and the porosity was calculated as $C = (m_3 - m_4)/1 \times 100\%$.[41] Three sets of individual samples were used for each new magnetic nanocomposite hydrogel, and the averages were used for all final analyses.

4.2.6.5. Infrared Spectroscopy. Each group of new magnetic nanocomposite hydrogels was cut into a sheet with a diameter of 12 mm and a height of approximately 2 mm and placed in a vacuum freeze-drying oven for 72 h to remove any residual water. Spectroscopic analysis was performed using an infrared spectrometer. Three sets of individual samples were used for each new magnetic nanocomposite hydrogel, and the averages were used for all final analyses.

4.2.6.6. In Vitro Degradation Experiments. Each group of new magnetic nanocomposite hydrogels was cut into a sheet with a diameter of 12 mm and a height of approximately 3 mm. Filter paper was used to remove any excess moisture on the surface of the hydrogels after which they were individually weighed using an electronic balance. The mass was recorded as m_5 after which samples were placed into 10 mL of PBS solution, and the solution was sealed and placed on a sway bed for uninterrupted vibration. The hydrogel sheets were removed weekly and weighed using an electronic balance, and the mass was recorded as m_6. The degradation rate was calculated as $C = (m_5 - m_6)/m_1 \times 100\%$.[41] Three sets of individual samples were used for each new magnetic nanocomposite hydrogel, and the averages were used for all final analyses.

4.2.6.7. CCK-8 Proliferation Experiment. Rabbit bone marrow mesenchymal stem cells obtained using the procedure outlined in section 4.2.3 were inoculated into the new magnetic nanocomposite hydrogels after the disinfection treatment outlined in section 4.2.4. The daily liquid exchange is shown in Figure S2C,D. CCK-8 proliferation assays were performed after 1, 3, and 7 days after inoculation. CCK-8 solution and DMEM medium were mixed evenly at a volume ratio of 1:10. The culture medium in the new magnetic nanocomposite hydrogels was discarded, and a mixture of 400 μL of CCK-8 solution and DMEM medium was then added. After incubating in a cell culture incubator for 4 h, a sterile micropipette was used to aspirate the culture medium to a 100 μL culture plate. This medium was then transferred to an unopened sterile 96-well plate after which absorption was measured at 450 nm using a microplate reader.

4.2.6.8. Living and Dead Cell Staining Experiments. Rabbit bone marrow mesenchymal stem cells were counted, and the cell density was adjusted to 1×10^6/ml. Columnar scaffolds with a diameter of 12 mm and a thickness of 3 mm were then prepared after which each scaffold was inoculated with a density of 1×10^6 cells. The cell/scaffold complex was placed in a 5% CO_2, 37 °C cell culture incubator, and the medium was changed every 3 days. After 7 days of culture, the cell/scaffold complex was removed for cell staining. Calcein AM and propidium iodide were prepared at a final concentration of 2 and 3 μM, respectively. The composite scaffold was stained using the aforementioned dyeing solutions and incubated at 37 °C for 30 min. All imaging were performed using fluorescence microscopy.

4.2.7. Data Analysis. The data obtained in this experiment were analyzed by SPSS21.0 software. The data between each sample group was analyzed by a chi-square test. It was statistically significant to set $P < 0.05$.

■ ASSOCIATED CONTENT

Supporting Information

The Supporting Information is available free of charge at https://pubs.acs.org/doi/10.1021/acsomega.9b04080.

Figure S1,S2, Methods and materials; Figure S3, discussion (PDF)

■ AUTHOR INFORMATION

Corresponding Authors

Jianghong Huang − *Shenzhen National Key Department of Orthopedics and Shenzhen Key Laboratory of Tissue*

https://dx.doi.org/10.1021/acsomega.9b04080
ACS Omega 2020, 5, 9733−9743

Engineering, Shenzhen Laboratory of Digital Orthopedic Engineering, Shenzhen Second People's Hospital (The First Hospital Affiliated to Shenzhen University), Shenzhen 518035, P. R China; orcid.org/0000-0002-8168-0081; Email: huangjianghong88@sohu.com

Daping Wang − *Shenzhen National Key Department of Orthopedics and Shenzhen Key Laboratory of Tissue Engineering, Shenzhen Laboratory of Digital Orthopedic Engineering, Shenzhen Second People's Hospital (The First Hospital Affiliated to Shenzhen University), Shenzhen 518035, P. R China*; Email: dapingwang1963@qq.com

Authors

Yujie Liang − *Shenzhen Kangning Hospital, Shenzhen Mental Health Center, Shenzhen, Guangdong Province 518020, P. R China*

Zhiwang Huang − *Shenzhen National Key Department of Orthopedics and Shenzhen Key Laboratory of Tissue Engineering, Shenzhen Laboratory of Digital Orthopedic Engineering, Shenzhen Second People's Hospital (The First Hospital Affiliated to Shenzhen University), Shenzhen 518035, P. R China*

Jianyi Xiong − *Shenzhen National Key Department of Orthopedics and Shenzhen Key Laboratory of Tissue Engineering, Shenzhen Laboratory of Digital Orthopedic Engineering, Shenzhen Second People's Hospital (The First Hospital Affiliated to Shenzhen University), Shenzhen 518035, P. R China*

Complete contact information is available at: https://pubs.acs.org/10.1021/acsomega.9b04080

Notes

The authors declare no competing financial interest.

■ ACKNOWLEDGMENTS

The authors acknowledge funding from Guangdong Province Science and Technology Project (grant no.2017A020215116), Shenzhen R & D funding project (JCYJ20160301111338144, JCYJ20170306092315034, JCYJ20180306170922163), Health and Family Planning Commission of Shenzhen Municipality project (SZXJ2018035), and Sanming project of medicine in Shenzhen (no. SZSM201612079).

■ REFERENCES

(1) Mohan, N.; Mohanan, P. V.; Sabareeswaran, A.; Nair, P. Chitosan-hyaluronic acid hydrogel for cartilage repair. *Int. J. Biol. Macromol.* **2017**, *104*, 1936.

(2) Zhou, Y.; Liang, K.; Zhao, S.; Zhang, C.; Li, J.; Yang, H.; Liu, X.; Yin, X.; Chen, D.; Xu, W.; Xiao, P. Photopolymerized maleilated chitosan/methacrylated silk fibroin micro/ nanocomposite hydrogels as potential scaffolds for cartilage tissue engineering. *Int. J. Biol. Macromol.* **2018**, *108*, 383.

(3) Hu, Y.; Liu, L.; Gu, Z.; Dan, W.; Dan, N.; Yu, X. Modification of collagen with a natural derived cross-linker, alginate dialdehyde. *Carbohydr. Polym.* **2014**, *102*, 324.

(4) Puttawibul, P.; Meesane, J.; Benjakul, S. Preparation and characterization of type I collagen/PVA hybrid biomimetic hydrogels scaffold for wound healing. *proceedings of the Biomedical Engineering International Conference.* 2013, *2012,* DOI: 10.1109/BMEiCon.2012.6465435.

(5) Ajalloueian, F.; Nikogeorgos, N.; Ajalloueian, A.; Fossum, M.; Lee, S.; Chronakis, I. S. Compressed collagen constructs with optimized mechanical properties and cell interactions for tissue engineering applications. *Int. J. Biol. Macromol.* **2017**, *108*, 158.

(6) Cutiongco, M. F.; Anderson, D. E.; Hinds, M. T.; Yim, E. K. In vitro and ex vivo hemocompatibility of off-the-shelf modified poly(vinyl alcohol) vascular grafts. *Acta Biomater.* **2015**, *25*, 97.

(7) Garcia-Lopez, J.; Garciadiego-Cázares, D.; Melgarejo-Ramirez, Y.; Sánchez-Sánchez, R.; Solís-Arrieta, L.; García-Carvajal, Z.; Sánchez-Betancourt, J. I.; Ibarra, C.; Luna-Bárcenas, G.; Velasquillo, C. Chondrocyte differentiation for auricular cartilage reconstruction using a chitosan based hydrogel. *Histol. Histopathol.* **2015**, *30*, 1477.

(8) Krych, A. J.; Wanivenhaus, F.; Ng, K. W.; Doty, S.; Warren, R. F.; Maher, S. A. Matrix generation within a macroporous non-degradable implant for osteochondral defects is not enhanced with partial enzymatic digestion of the surrounding tissue: evaluation in an in vivo rabbit model. *J. Mater. Sci.: Mater. Med.* **2013**, *24*, 2429.

(9) Gohil, S. V.; Wang, L.; Rowe, D. W.; Nair, L. S. Spatially controlled rhBMP-2 mediated calvarial bone formation in a transgenic mouse model. *Int. J. Biol. Macromol.* **2018**, *106*, 1159.

(10) Liu, L.; Wen, H.; Rao, Z.; Zhu, C.; Liu, M.; Min, L.; Fan, L.; Tao, S. Preparation and characterization of chitosan-collagen peptide/ oxidized konjac glucomannan hydrogel. *Int. J. Biol. Macromol.* **2017**, *108*, 376.

(11) Shao, R. X.; Quan, R. F.; Wang, T.; Du, W. B.; Jia, G. Y.; Wang, D.; Lv, L. B.; Xu, C. Y.; Wei, X. C.; Wang, J. F.; Yang, D. S. Effects of a bone graft substitute consisting of porous gradient HA/ZrO2 and gelatin/chitosan slow-release hydrogel containing BMP-2 and BMSCs on lumbar vertebral defect repair in rhesus monkey. *J. Tissue Eng. Regener. Med.* **2018**, *12*, No. e1813.

(12) Ghorbani, M.; Ai, J.; Nourani, M. R.; Azami, M.; Hashemi Beni, B.; Asadpour, S.; Bordbar, S. Injectable natural polymer compound for tissue engineering of intervertebral disc: In vitro study. *Mater. Sci. Eng. C* **2017**, *80*, 502.

(13) Moulisová, V.; Poveda-Reyes, S.; Sanmartín-Masiá, E.; Quintanilla-Sierra, L.; Salmerón-Sánchez, M.; Gallego Ferrer, G. Hybrid Protein-Glycosaminoglycan Hydrogels Promote Chondrogenic Stem Cell Differentiation. *ACS Omega.* **2017**, *2*, 7609.

(14) Mahoney, C. M.; Kelmindi-Doko, A.; Snowden, M. J.; Peter Rubin, J.; Marra, K. G. Adipose derived delivery vehicle for encapsulated adipogenic factors. *Acta Biomater.* **2017**, *58*, 26.

(15) Kaneko, A.; Matsushita, A.; Sankai, Y. A 3D nanofibrous hydrogel and collagen sponge scaffold promotes locomotor functional recovery, spinal repair, and neuronal regeneration after complete transection of the spinal cord in adult rats. *Biomed. Mater.* **2015**, *10*, No. 015008.

(16) Paduano, F.; Marrelli, M.; White, L. J.; Shakesheff, K. M.; Tatullo, M. Odontogenic Differentiation of Human Dental Pulp Stem Cells on Hydrogel Scaffolds Derived from Decellularized Bone Extracellular Matrix and Collagen Type I. *PLoS One* **2016**, *11*, No. e0148225.

(17) Yuan, L.; Wu, Y.; Gu, Q. S.; El-Hamshary, H.; El-Newehy, M.; Mo, X. Injectable photo crosslinked enhanced double-network hydrogels from modified sodium alginate and gelatin. *Int. J. Biol. Macromol.* **2017**, *96*, 569.

(18) Kimura, A.; Kabasawa, Y.; Tabata, Y.; Aoki, K.; Ohya, K.; Omura, K. Gelatin hydrogel as a carrier of recombinant human fibroblast growth factor-2 during rat mandibular distraction. *J. Oral Maxillofac. Surg.* **2014**, *72*, 2015.

(19) Wang, L.; Lai, D. M.; Yang, B.; Jiang, Z. P.; Zhang, Y. C.; Zhou, J.; Lai, W.; Chen, S. Reconstruction of abdominal wall defects using small intestinal submucosa coated with gelatin hydrogel incorporating basic fibroblast growth factor. *Acta cirurgica brasileira.* **2014**, *29*, 252.

(20) Thorpe, A. A.; Boyes, V. L.; Sammon, C.; Le Maitre, C. L. Thermally triggered injectable hydrogel, which induces mesenchymal stem cell differentiation to nucleus pulposus cells: Potential for regeneration of the intervertebral disc. *Acta Biomater.* **2016**, *36*, 99.

(21) Shamloo, A.; Sarmadi, M.; Aghababaie, Z.; Vossoughi, M. Accelerated full-thickness wound healing via sustained bFGF delivery based on a PVA/chitosan/gelatin hydrogel incorporating PCL microspheres. *Int. J. Pharm.* **2018**, *537*, 278.

(22) Maya, S.; Sarmento, B.; Nair, A.; Rejinold, N. S.; Nair, S. V.; Jayakumar, R. Smart stimuli sensitive nanogels in cancer drug delivery and imaging: a review. *Curr. Pharm. Des.* **2013**, *19*, 7203.
(23) Hu, X.; Wang, Y.; Zhang, L.; Xu, M.; Zhang, J.; Dong, W. Magnetic field-driven drug release from modified iron oxide-integrated polysaccharide hydrogel. *Int. J. Biol. Macromol.* **2018**, *108*, 558.
(24) Wang, H.; Liang, Y.; Gao, W.; Dong, R.; Wang, C. Emulsion Hydrogel Soft Motor Actuated by Thermal Stimulation. *ACS Appl. Mater. Interfaces* **2017**, *9*, 43211.
(25) Kesavan, M. P.; Ayyanaar, S.; Lenin, N.; Sankarganesh, M.; Dhaveethu Raja, J.; Rajesh, J. One pot synthesis of new poly(vinyl alcohol) blended natural polymer based magnetic hydrogel beads: Controlled natural anticancer alkaloid delivery system. *J. Biomed. Mater. Res., Part A* **2018**, *106*, 543.
(26) Brady, M. A.; Talvard, L.; Vella, A.; Ethier, C. R. Bio-inspired design of a magnetically active trilayered scaffold for cartilage tissue engineering. *J. Tissue Eng. Regener. Med.* **2017**, *11*, 1298.
(27) Zhang, N.; Lock, J.; Sallee, A.; Liu, H. Magnetic nanocomposite hydrogel for Potential Cartilage Tissue Engineering: Synthesis, Characterization, and Cytocompatibility with Bone Marrow Derived Mesenchymal Stem Cells. *ACS Appl. Mater. Interfaces* **2015**, *7*, 20987.
(28) Lee, K. Y.; Mooney, D. J. Hydrogels for Tissue Engineering. *Chem. Rev.* **2001**, *101*, 1869.
(29) Hoffman, A. S. Hydrogels for Biomedical Applications. *Ann. N. Y. Acad. Sci.* **2002**, *944*, 3.
(30) Heo, J.; Koh, R. H.; Shim, W.; Kim, H. D.; Yim, H. G.; Hwang, N. S. Riboflavin-induced photo-crosslinking of collagen hydrogel and its application in meniscus tissue engineering. *Drug Delivery Transl. Res.* **2016**, *6*, 148.
(31) Zhang, X.; Xu, L.; Huang, X.; Wei, S.; Zhai, M. Structural study and preliminary biological evaluation on the collagen hydrogel crosslinked by gamma-irradiation. *J. Biomed. Mater. Res., Part A* **2012**, *100*, 2960.
(32) Zheng, L.; Lu, H. Q.; Fan, H. S.; Zhang, X. D. Reinforcement and chemical cross-linking in collagen-based scaffolds in cartilage tissue engineering: a comparative study. *Iran. Polym. J.* **2013**, *22*, 833.
(33) Filippi, M.; Dasen, B.; Guerrero, J.; Garello, F.; Isu, G.; Born, G.; Ehrbar, M.; Martin, I.; Scherberich, A. Magnetic nanocomposite hydrogels and static magnetic field stimulate the osteoblastic and vasculogenic profile of adipose-derived cells. *Biomaterials* **2019**, *223*, 119468.
(34) Huang, J.; Liang, Y.; Huang, Z.; Zhao, P.; Liang, Q.; Liu, Y.; Duan, L.; Liu, W.; Zhu, F.; Bian, L.; Xia, J.; Xiong, J.; Wang, D. Magnetic Enhancement of Chondrogenic Differentiation of Mesenchymal Stem Cells. *ACS Biomater. Sci. Eng.* **2019**, *5*, 2200.
(35) Huang, J.; Liu, W.; Liang, Y.; Li, L.; Duan, L.; Chen, J.; Zhu, F.; Lai, Y.; Zhu, W.; You, W.; Jia, Z.; Xiong, J.; Wang, D. Preparation and Biocompatibility of Diphasic Magnetic Nanocomposite Scaffold Materials. *Mater. Sci. Eng. C* **2018**, *87*, 70.
(36) Huang, J.; Liang, Y.; Jia, Z.; Chen, J.; Duan, L.; Liu, W.; Zhu, F.; Liang, Q.; Zhu, W.; You, W.; Xiong, J.; Wang, D. Development of Magnetic nanocomposite hydrogel with Potential Cartilage Tissue Engineering. *ACS Omega* **2018**, *3*, 6182.
(37) Huang, J.; Jia, Z.; Liang, Y.; Huang, Z.; Rong, Z.; Xiong, J.; Wang, D. Pulse electromagnetic fields enhance the repair of rabbit articular cartilage defects with magnetic nano-hydrogel. *RSC Adv.* **2020**, *10*, 541.
(38) Yang, W.; Zhu, P.; Huang, H.; Zheng, Y.; Liu, J.; Feng, L.; Guo, H.; Tang, S.; Guo, R. Functionalization of Novel Theranostic Hydrogels with Kartogenin-Grafted USPIO Nanoparticles To Enhance Cartilage Regeneration. *ACS Appl. Mater. Interfaces* **2019**, *11*, 34744.
(39) Bonhome-Espinosa, A. B.; Campos, F.; Durand-Herrera, D.; Sánchez-López, J. D.; Schaub, S.; Durán, J. D. G.; Lopez-Lopez, M. T.; Carriel, V. In vitro characterization of a novel magnetic fibrin-agarose hydrogel for cartilage tissue engineering. *J. Mech. Behav. Biomed. Mater.* **2020**, *104*, 103619.
(40) Chen, C. H.; Kuo, C. Y.; Wang, Y. J.; Chen, J. P. Dual Function of Glucosamine in Gelatin/Hyaluronic Acid Cryogel to Modulate Scaffold Mechanical Properties and to Maintain Chondrogenic Phenotype for Cartilage Tissue Engineering. *Int. J. Mol. Sci.* **2016**, *17*, 1957.
(41) Huang, D.; Wang, R.; Yang, S. Cogels of Hyaluronic Acid and Acellular Matrix for Cultivation of Adipose-Derived Stem Cells: Potential Application for Vocal Fold Tissue Engineering. *BioMed Res. Int.* **2016**, *2016*, 6584054.

https://dx.doi.org/10.1021/acsomega.9b04080
ACS Omega 2020, 5, 9733−9743